Journal of
Materials Chemistry B

PAPER

View Article Online
View Journal | View Issue

Cite this: J. Mater. Chem. B, 2015, 3, 8410

Hemocompatible, antioxidative and antibacterial polypropylene prepared by attaching silver nanoparticles capped with TPGS†

Chunming Li,[ab] Bing Cai,[a] Jing Jin,*[a] Jingchuan Liu,[a] Xiaodong Xu,[c] Jinghua Yin*[a] and Ligang Yin[d]

Infections associated with medical devices cause significant costs, morbidity, and mortality. Medical devices with hemocompatibility, antioxidative stress, and antibacterial properties are difficult to fabricate. In this study, silver nanoparticles (Ag NPs) were synthesized for the first time in the presence of carboxylic D-α-tocopheryl polyethylene glycol 1000 succinate (TPGS) as antibacterial agents. The Ag NPs were characterized by UV-visible spectroscopy, transmission electron microscopy, and zeta potential measurements. The results showed that Ag NPs had a good dispersion stability and uniform size distribution. The introduction of TPGS dispersed the Ag NPs in solution and provided active protection against Ag NP-induced free radical damage. *N*-Isopropylacrylamide (NIPAAm) and *N*-(3-aminopropyl) methacrylamide hydrochloride (APMA) were then co-grafted onto polypropylene (PP) membranes by ultraviolet grafting, which can provide antifouling properties. The modified PP surface can be used as a platform to load the Ag NPs capped with TPGS. The loading efficiency of Ag NPs was mediated by electrostatic interactions between the positively charged APMA and the negatively charged Ag NPs. The loaded TPGS can slow the lipid peroxidation of erythrocytes and fill the lipid bilayer of erythrocytes to prevent antioxidative stress and hemolysis. The bacteria adhesion, bacterial activity, and biofilm formation proved that the modified PP surfaces loaded with Ag NPs had excellent antibacterial and bactericidal properties. Therefore, our approach can serve as a basis for developing medical devices with excellent hemocompatibility, as well as simultaneous antioxidative and antibacterial properties, thereby providing a potential prevention measure of medical-device-associated infections.

Received 1st August 2015,
Accepted 16th September 2015

DOI: 10.1039/c5tb01554e

www.rsc.org/MaterialsB

1. Introduction

Medical-device-associated infections remain a major hindrance to the long-term use of medical devices.[1] Antifouling and antibacterial coatings have been applied as two of the most promising strategies to protect blood cells and kill bacteria. Hemocompatibility, as well as oxidative stress and antibacterial properties, limit the using of blood-contacting medical devices, such as heart valves, catheters, pacemaker leads, hemodialysis membranes, and blood storage devices.[2] Hemolysis and thrombus formation are two major complications that affect the hemocompatibility of blood-contacting medical devices. Thrombus formation increases the risk of vascular occlusion and potential thrombus embolization, which may result in tissue damage or stroke.[3] Hemolysis stands for the rupture of red blood cells (RBCs) with the releasing of hemoglobin into the suspending medium, which may lead to organ failure and patient death during blood transfusion.[4] The accumulation of lipid peroxidation of the RBC membrane causes membrane damage during storage and transport, which could decrease membrane integrity and flexibility, thereby leading to hemolysis. Erythrocytes are frequently used to investigate the potential activity of antioxidants because of the high levels of polyunsaturated fatty acids in their membranes.[5] An excess of reactive oxygen species (ROS) causes damage to cell components; this effect is another important issue for blood-contacting devices.[6]

ROS are largely produced by neutrophils and monocytes through protein and lipid oxidation. ROS-inducing hemolysis is controlled by some scavengers of oxygen-derived radicals, such

[a] State Key Laboratory of Polymer Physics and Chemistry, Changchun Institute of Applied Chemistry, Chinese Academy of Sciences, Changchun 130022, P. R. China. E-mail: jjin@ciac.ac.cn, yinjh@ciac.ac.cn; Fax: +86-431-85262126; Tel: +86-431-85262109
[b] University of Chinese Academy of Sciences, Beijing 100049, P. R. China
[c] Polymer Materials Research Center, College of Materials Science and Chemical Engineering, Harbin Engineering University, Harbin 150001, P. R. China
[d] Wego Holding Company Limited, Weihai 264200, P. R. China

† Electronic supplementary information (ESI) available: Quantitative data of fluorescence intensity on the surface, SEM analysis of erythrocytes, bacterial adhesion, biofilm formation and bactericidal activity of *S. aureus*. See DOI: 10.1039/c5tb01554e

as *N*-allylsecoboldine,[7] *c*-phycocyanin,[5] epicatechin,[8,9] tea polyphenols,[10] and vitamin E.[11] Vitamin E is one of the materials that can improve the antioxidative activity of hemodialysis membranes.[12,13] D-α-Tocopheryl polyethylene glycol 1000 succinate (TPGS) is formed by the esterification of vitamin E succinate with polyethylene glycol (PEG) 1000, which is a water-soluble vitamin E formulation. TPGS has been approved by the U.S. Food and Drug Administration as a safe pharmaceutical adjuvant in drug formulation.[14] Bellare *et al.* fabricated a polysulfone membrane containing TPGS in a single step with enhanced biocompatibility, high flux, and urea clearance.[6] Feng *et al.* synthesized a series of novel copolymers by TPGS for the nanoparticle formulation of anticancer drugs.[15–18] TPGS is clearly an amphiphile with a PEG oligomer of significant length and a 16-carbon alkyl chain, but, to the best of our knowledge, the compound has not been used as a metal nanomaterial dispersant.

Medical-device-associated infections have caused significant morbidity, mortality and additional costs. Infection starts with bacterial adhesion, bacterial colonization followed by the formation of biofilms that serve as reservoirs for the development of pathogenic infections.[19,20] Antibacterial surfaces are urgently needed for blood-contacting devices. Several methods have been used to test and assay biomaterial-associated infections. Non-fouling surfaces, which are also called adhesion resistant surfaces, can reduce the adhesion of bacteria onto surfaces. Recently, polymer brushes have attracted considerable attention as a method to engineer the surface properties of materials.[21] As protein molecules or bacteria compress the hydrated polymer brush layer on a biomaterial surface, the increased osmotic pressure within the brush and the decrease in the conformational entropy of the grafted polymer chains make them repel the adhesion of proteins and bacteria. Unfortunately, only a few adherent bacteria are required to form a mature biofilm.[22] Therefore, a combination of both approaches should produce effective antibacterial coatings by reducing the initial cell adhesion by non-adhesive properties and killing bacteria adhered onto the surface by the simultaneous presence of a biocidal substance. Incorporating antibiotics into a surface is an effective strategy to kill bacteria or prevent their growth; these antibiotics include rifampicin,[23,24] gentamycin,[25] minocycline,[26] and fusidic acid.[27] However, these compounds are associated with the development of antibiotic resistance.[28] Bacteriophages (phages) are viruses of bacteria that can kill and lyse the bacteria they infect.[29] Although there are still several problems to be solved, the potential is that phage therapy will regain a role in treatments of both veterinary and medical infectious diseases. An increasing amount of literature has validated the use of bacteriophages for therapy and prophylaxis against drug-resistant staphylococci.[30,31] Silver ions have been used as antibacterial agents since ancient times, whereas the use of silver nanoparticles (Ag NPs) as antibacterial agents has become very important in recent years.[32–34] The Ag NPs used in previous studies are believed to be less cytotoxic based on the mass of silver added.[35] However, Ag NPs that entered into mammalian cells and altered the intracellular functions adversely were toxic at a high dosage. It is believed that Ag NP surfaces can readily dissolve in aqueous solution to generate Ag^+, which can lead to cell damage either indirectly, by generating reactive oxygen species that cause oxidative stress, or directly, by reacting with cellular amino and thiol groups of proteins within cell membranes.[36,37] The Food and Drug Administration (FDA) ceased the clinical investigations of the St Jude heart valve based on absence of tissue integration. Besides, the mechanism of the antibacterial effect of Ag NPs remains uncertain.[38,39] It is significant to explore and understand the surface structure of Ag NPs, which will provide insight into the antibacterial activity.

An appropriate coating of Ag NPs surfaces is required in biological applications to avoid their aggregation in highly saline media and favor their solubility in water-based environments.[40] The synthesis of Ag NPs in the presence of coating agents, such as collagen,[41] sodium dodecyl sulfate (SDS),[42] ceragenin,[43] and glutathione,[44] has shown a better antimicrobial activity. However, the combination of amphipathic and antioxidant TPGS to fabricate Ag NPs has not been reported. TPGS can develop the application potential and reduce the toxic effects of Ag NPs.

Previous work reported[45] the loading of TPGS onto *N*-isopropylacrylamide (NIPAAm) and *N*-(3-aminopropyl) methacrylamide hydrochloride (APMA) co-grafted polypropylene (PP-P (NIPAAm-*co*-APMA)); the modified PP showed excellent hemocompatibility and antioxidative properties. In addition, the interaction mechanism between the release of TPGS and erythrocytes was proposed. In the present work, we report a novel method to synthesize Ag NPs as coating agents in the presence of TGPS. The positive charge of APMA presented on the grafting brushes serve as anchoring points for the attachment of Ag NPs and TPGS, which simultaneously endowed PP with hemocompatibility, as well as antioxidative and efficient antibacterial activity. The proposed method may be a convenient and easy approach to fabricate biomaterials for use in complex environments.

2. Experimental section

2.1 Materials

Polypropylene nonwoven fabric (PP NWF) membranes were obtained from Beijing JDKR Co., Ltd (Beijing, China) with an average pore diameter of 0.22 μm. *N*-(3-Aminopropyl)-methacrylamide hydrochloride (APMA), *N*-isopropylacrylamide (NIPAAm), D-α-tocopherol polyethylene glycol 1000 succinate (TPGS), succinic anhydride (SA), 4-(dimethylamino)pyridine (DMAP) and triethylamine (TEA) were purchased from Sigma-Aldrich Chemical Co. Silver nitrate ($AgNO_3$) and sodium borohydride ($NaBH_4$) were obtained from J&K Chemical Ltd. Fluorescein-isothiocyanate-labelled fibrinogen (FITC-Fib) was obtained from Bioss Inc. Gram-negative *Escherichia coli* (*E. coli*; ATCC 25922) and Gram-positive *Staphylococcus aureus* (*S. aureus*; ATCC 6538), Luria-Bertani (LB) broth, trypticase soy broth (TSB) and phosphate-buffered saline (PBS, 0.01 M phosphate buffer, pH 7.4) were obtained from Dingguo Biotechnology Co., Ltd. The other reagents and solvents were AR grade and used without further purification.

2.2 Preparation and characterization of Ag NPs

2.2.1. Synthesis of carboxyl-terminated TPGS. TPGS was activated by succinic anhydride to introduce a negative charge to TPGS through a ring-opening reaction in the presence of DMAP, according to the study of Si-Shen Feng[15] and our previous work.[46] Succinic anhydride (0.6 mmol), TPGS (0.5 mmol), DMAP (0.5 mmol), and TEA (0.5 mmol) were dissolved in anhydrous dioxane (6 mL) and stirred at 40 °C for 24 h. An ester bond was formed here between the hydroxyl-terminated TPGS and the carboxylic group of succinic anhydride. The solvent was evaporated completely in a rotary evaporator. The white residue was dissolved in dichloromethane and then filtered to remove unreacted succinic anhydride. The solution was precipitated in anhydrous ether after filtration. The precipitated product, carboxyl-terminated TPGS (TPGS-SA), was then freeze-dried. TPGS used to synthesize Ag NPs represents a carboxyl-terminated TPGS in this article, if not stated otherwise.

2.2.2 Preparation of Ag NPs. Some researchers synthesized Ag NPs between 3 and 5 nm by using $AgNO_3$, $NaBH_4$ and sodium citrate tribasic dehydrate.[47,48] Here, Ag NPs were prepared by chemically reducing $AgNO_3$ with $NaBH_4$ in the presence of TPGS. Briefly, aqueous solutions of $AgNO_3$ and TPGS were mixed under vigorous stirring for 3 min. Then, $NaBH_4$, pre-dissolved in water, was added dropwise under vigorous stirring to this solution at room temperature, resulting in a yellowish brown Ag hydrosol. In this work, Ag NPs were prepared at three different concentrations of $AgNO_3$, 2, 1, and 0.5 mM, while keeping the final amount of TPGS and the molar ratios of $AgNO_3$ and $NaBH_4$ constant. Sample 1 (χ_{Ag} = 0.5 mM, Ag(0.5)NP) was prepared by $AgNO_3$, $NaBH_4$ and TPGS at final concentrations of 0.5 and 0.6 mM, and 0.05 wt%, respectively. Sample 2 (χ_{Ag} = 1.0 mM, Ag(1.0)NP) was prepared by $AgNO_3$, $NaBH_4$ and TPGS at final concentrations of 1.0 and 1.2 mM, and 0.05 wt%, respectively. Sample 3 (χ_{Ag} = 2.0 mM, Ag(2.0)NP) was prepared by $AgNO_3$, $NaBH_4$ and TPGS at final concentrations of 2.0 and 2.4 mM, and 0.05 wt%, respectively.

2.2.3 Ag nanoparticle characterization

Transmission electron microscopy (TEM). Ag NPs prepared in this study were characterized using a field emission microscope (JEOL JEM1011, Japan) at an operating voltage of 200 kV. The observed samples were prepared by dropping 10 μL of the nanoparticle colloid dispersion on a 3 mm carbon-coated copper grid. Excess solution was removed and the drop was dried in air at room temperature. The size and shape distribution of the nanoparticles were characterized by TEM. The size distribution of nanoparticles was measured using histograms from the TEM images. Statistical analysis was performed by one-way ANOVA to determine the differences in nanoparticle sizes.

Ultraviolet-visible (UV-Vis) analysis. The synthesized nanoparticles were analyzed by using a UV-vis spectrophotometer (PerkinElmer Lambda 35, America) with a wave-number range between 300 and 700 nm. Before the measurements, nanoparticle solutions were diluted 90-fold with deionized water.

Zeta potential measurements. The zeta potential of Ag NP suspensions was measured with a Zetasizer Nano-ZS instrument (Malvern Instruments Ltd, UK).

2.3 Preparation, characterization, and hemocompatibility of modified PP membranes

2.3.1. Preparation of APMA- and NIPAAm-modified responsive polymer brushes. Details of the preparation and characterization of NIPAAm and APMA polymer brushes on the PP surface had been described earlier.[41] Briefly, PP NWF membranes of 1 cm × 2 cm in size were cleaned with acetone for 30 min in an ultrasonic water bath. The films were dried under vacuum at 25 °C for 24 h. The dry PP membranes were immersed in the 1 wt% BP-ethanol solution for 30 min and then dried at 25 °C. Then the PP membranes were put on a quartz plate and 50 μL of APMA and NIPAAm aqueous solution dropped onto them. The membrane was then covered with another quartz plate. The resulting sandwiched system was exposed to UV light (main wavelength = 380 nm, high-pressure mercury lamp, 400 W) for the desired period. Finally, the grafting membranes were washed with ethanol and water continuously to remove ungrafted monomer. The chemical compositions of the modified PP membranes were characterized by X-ray photoelectron spectroscopy (XPS, VG Scientific ESCA MK II Thermo Avantage V 3.20 analyzer) with an Al/K ($h\nu$ = 1486.6 eV) anode mono-X-ray source. The surface chemical structure of the modified PP membranes was analyzed by Fourier transform infrared spectroscopy (FTIR, BRUKER Vertex 70) with an attenuated total reflection unit (ATR crystal, 45°) at a resolution of 4 cm^{-1} for 32 scans.

2.3.2. Deposition of Ag NPs on PP NWF surfaces. Virgin control PP and PP-*g*-P(NIPAAm-*co*-APMA) with different mole ratios of NIPAAm and APMA on their surface were incubated for 12 h at 25 °C in Ag NP colloidal dispersion with a molar concentration of 0.5 mM. The process led to adsorption of TPGS and Ag NPs on the grafting PP surfaces. The resultant membranes were rinsed with DI water continuously.

2.3.3 FITC-Fib absorption test. The pieces of the membranes were washed by PBS three times and placed in a tissue culture plate. Then 20 μL of 60 μg mL^{-1} FITC-Fib was dropped onto the center of the membrane and incubated for 120 min at 37 °C. The physically absorbed protein was rinsed with water three times. After rinsing, substrate-immobilized protein was imaged by confocal laser scanning microscopy (CLSM, Carl Zeiss LSM 700, Germany).

2.3.4 Blood-clotting test. Fresh blood gathered from a healthy adult rabbit was mixed immediately with a 3.8 wt% solution of sodium citrate at a dilution ratio of 9 : 1. (The experiments were carried out in accordance with the guidelines issued by the Ethical Committee of the Chinese Academy of Sciences.) Then, the blood was centrifuged for 15 min at 1000 rpm to obtain the platelet-rich plasma (PRP). Membranes pieces (2 cm × 2 cm) were immersed in PBS for 2 h and placed in a clean tissue culture plate. Then 20 μL of PRP was put onto the center of the membrane and incubated for 60 min at 37 °C. The physically adhered platelets were rinsed by PBS three times. Soon afterwards, the platelets that adhered onto the membrane were fixed by 2.5 wt% glutaraldehyde for 12 h at 4 °C. Finally, the membranes were washed with PBS, dehydrated with a series of water/ethanol mixtures (30, 50, 70, 90, and 100 vol% ethanol; 15 min for each mixture), and finally dried under vacuum. The surface

of the membrane was gold-sputtered in vacuum and observed with field emission scanning electron microscopy (FESEM, XL 30 ESEM FEG, FEI Company).

2.3.5 Hemolysis rate test. Blood from the rabbit was collected in tubes containing sodium citrate and used within 4 h. Erythrocytes were separated from the plasma and lymphocytes by centrifugation (3000*g*, 5 min) at 4 °C, washed three times with PBS and suspended in PBS. Grafting and loading PP membranes were immersed in 3 mL of erythrocyte PBS suspensions. The samples were incubated on a thermostatic shaker for a certain time (12 h, 24 h and 36 h) at 37 °C, 130 r min^{-1}. Negative and positive controls were prepared by adding 30 μL of erythrocytes to 3 mL of PBS and distilled water, respectively. After incubation, suspensions were centrifuged (800*g*, 5 min). The optical density of the supernatant was measured at 541 nm. The percent hemolysis was calculated as follows:

$$\text{Hemolysis (\%)} = [(OD_{sam} - OD_{neg})/(OD_{pos} - OD_{neg})] \times 100$$

where OD_{sam}, OD_{neg}, and OD_{pos} are the absorbance values of the test sample, negative control (saline) and positive control (water), respectively. The hemolysis experiments were done simultaneously three times.

For investigating the morphological changes, erythrocytes at the end of the incubation period of the test samples were fixed in 2.5% glutaraldehyde for 60 min and washed three times with PBS. Cells were dehydrated with a series of water/ethanol mixtures (30, 50, 70, 90, and 100 vol% ethanol) for 15 min each. The cell pellets were dropped onto glass coverslips, dried and observed by confocal laser scanning microscopy (CARL ZEISS LSM 700, Germany). Besides, the samples were gold-sputtered in vacuum before viewing under field emission scanning electron microscopy (FESEM, XL 30 ESEM FEG, FEI Company).

2.4 Antibacterial activities of PP NWF with loaded Ag NPs

The adhesion and antibacterial activities of *E. coli* and *S. aureus* cells were studied on PP, PP-*g*-P(NIPAAm) and PP-*g*-P(NIPAAm-*co*-APMA) with the mole ratios of NIPAAm and APMA ($M_{NIPAAm:APMA}$) = 2 : 1, 5 : 1 and 10 : 1, and the corresponding Ag NP-treated PP. *E. coli* and *S. aureus* were inoculated onto agar plates, and incubated overnight at 37 °C. A single colony of *E. coli* or *S. aureus* from the agar plate was used to inoculate 10 mL of LB and cultured for 24 h at 37 °C and 120 rpm. The bacterial cell concentration was calculated by testing the absorbance of cell dispersions at 540 nm relative to a standard calibration curve. An optical density of 0.1 at 540 nm is equivalent to ~ 10^8 cells per mL.

2.4.1 Bacteria adhesion test. After removing the supernatant, the bacterial cells were diluted with PBS to 10^8 cells per mL. The samples were placed in 24-well plates and 500 μL of bacterial cells was dropped onto the surface of the samples at 37 °C for 2 h. Non-adherent bacteria were rinsed off by gently washing with PBS. Subsequently, the bacteria adhering to the membrane were fixed by 4 wt% paraformaldehyde at room temperature for 30 min. Finally, the conducted membranes were washed with PBS three times and freeze-dried. The surface of the membrane was gold-sputtered in a vacuum and observed with field emission scanning electron microscopy (SEM, XL-30 ESEM FEG, FEI Company).

2.4.2 Shaking flask method. After removing the supernatant, the bacterial cells were diluted with PBS to 10^8 cells per mL. The samples were placed in 24-well plates and 10 μL of bacterial cells was dropped onto the surface of the samples at 37 °C for 2 h. Non-adherent bacteria were rinsed off by gently washing with PBS. After that, ultrasonic treatment (3 min) was applied to the samples in 0.5 mL PBS aliquots. Finally, a 30 μL volume of the suspension was taken out and plated on gelatinous LB agar plates. The agar plates were incubated for 18 h at 37 °C, and the number of viable bacteria on the plates was counted as colony forming units (CFU) at the end of the incubation period.

2.4.3 Biofilm formation. Bacterial cells were diluted with LB to 10^6 cells per mL. The samples were placed in 24-well plates and 500 μL of a bacterial cell LB solution was dropped onto the surface of the samples at 37 °C for 24 h. Non-adherent bacteria were rinsed off by gently washing with PBS. Subsequently, the bacteria adhering to the membrane were fixed by 4 wt% paraformaldehyde at 4 °C for 10 h. Finally, the membranes were washed with PBS three times and then freeze-dried. The surface of the membrane was gold-sputtered in vacuum and observed with field emission scanning electron microscopy (FESEM, XL 30 ESEM FEG, FEI Company).

3. Results and discussion

3.1 Preparation and characterization of Ag NPs

Ag NPs have been synthesized in the presence of an appropriate coating of the NP surface to avoid their aggregation in highly saline media. TPGS is clearly an amphiphile with potential applications in dispersing NPs. In the present study, Ag NPs were synthesized in the present of TPGS for the first time (Scheme 1). According to our previous work, TPGS is activated by succinic anhydride *via* a ring-opening reaction to introduce negative charges in the presence of DMAP.[45] The UV-visible spectra of Ag NPs synthesized at three different concentrations are shown in Fig. 1. The strong and symmetrical absorption at 406 nm is caused by the excitation of surface plasmon resonance (SPR) in the Ag NPs, which indicates the small and uniform nanoparticle size distribution.[49] Homogenously dispersed Ag NPs in glass containers demonstrate a distinct gradient of colors, which corresponds to the different concentrations of Ag NPs (inset photograph in Fig. 1). The control reaction was performed in DI water without TPGS. A stable colloidal suspension of Ag NPs could not form when TPGS was

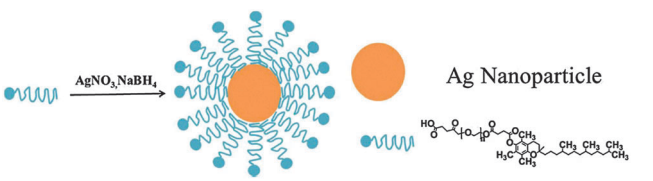

Scheme 1 Schematic plot of preparing TPGS conjugated Ag NPs.

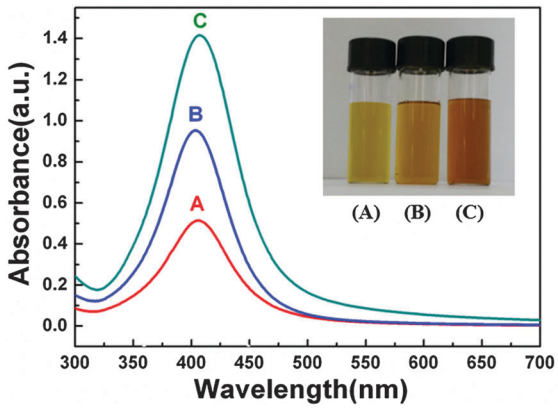

Fig. 1 UV-visible spectra of silver nanoparticles prepared in aqueous solutions at three different molar concentrations of $AgNO_3$: (A) χ_{Ag} = 0.5 mM, (B) χ_{Ag} = 1.0 mM and (C) χ_{Ag} = 2.0 mM. The inset shows the photographs of solutions containing Ag NPs synthesized with different molar concentrations of $AgNO_3$: (A) χ_{Ag} = 0.5 mM, (B) χ_{Ag} = 1.0 mM and (C) χ_{Ag} = 2.0 mM.

not in the solution. Similar to the pioneering experimental results, the solution color gradually changed from yellow to brown after the addition of silver nitrate; metallic Ag was observed to be stuck on the stirring bar and the beaker.[50] The solution is stable for more than three months when stored in a closed vial. Transmission electron microscopy (TEM) images of Ag NPs at different concentration and the respective size distribution histograms are shown in Fig. 2. The particles are nearly spherical in shape. The average size and size distribution of the Ag NPs were determined by analyzing at least 200 NPs. The average size of the NPs is 6–8 nm and the mean size did not noticeably change with increasing molar concentrations of $AgNO_3$. The zeta potential of the NPs synthesized with χ_{Ag} = 0.5 mM was -37.3 ± 9.3 mV, which is above the established ± 30 mV threshold for colloidal stability. These results indicate that the adsorption of anionic TPGS could render a surface negative charge (Scheme 1).

The antimicrobial effects of Ag nanomaterials are not widely understood or agreed upon. The commonly proposed mechanisms in the literature begin with the release of silver ions,[51] followed by the generation of ROS[52] and cell membrane damage. However, excess ROS may damage blood cells, which is another important issue for blood-contacting devises. The antioxidant function of TPGS can provide active protection against the Ag NP-induced free-radical damage. In addition, the stability of Ag NPs influences the toxicity because aggregate formation tends to decrease biocidal activity. The amphiphile of TPGS causes Ag NPs to disperse well in solution. The above-mentioned results confirm that the amphiphile, with its antioxidant functions and commercial availability, makes TPGS an attractive potential synthetic surfactant for the green processing of Ag NPs.

3.2 Adsorption of Ag NPs on a grafted PP surface

In our previous work,[45] NIPAAm and APMA were co-grafted onto the surface of PP. The chemical component of grafted PP was systematically characterized by ATR-FTIR and XPS. Grafted cationic APMA significantly promoted the uptake of anionic molecules and electrostatically interacted with anionic molecules for controlled release. Therefore, PP-*g*-P (NIPAAm) and PP-*g*-P(NIPAAm-*co*-APMA) with different $M_{NIPAAm:APMA}$ were used for the adsorption of Ag NPs. Fig. 3 shows the SEM micrographs of modified PP after Ag NP adsorption. The adsorption was evidenced by a prominent color that appeared on PP surfaces.[53] The color changed from white to yellow after the adsorption of Ag NPs for co-grafted PP. The color of the sample with $M_{NIPAAm:APMA}$ = 2 : 1 is deeper than that of the other samples because of the large amount of APMA on the surface. The Ag NPs are almost absent on the surface of PP-*g*-P (NIPAAm) in the SEM micrographs. By contrast, Ag NPs are clearly visible on the surface of PP-*g*-P(NIPAAm-*co*-APMA). The prepared Ag NPs are negatively charged, whereas the grafted PP is positively charged, such that numerous

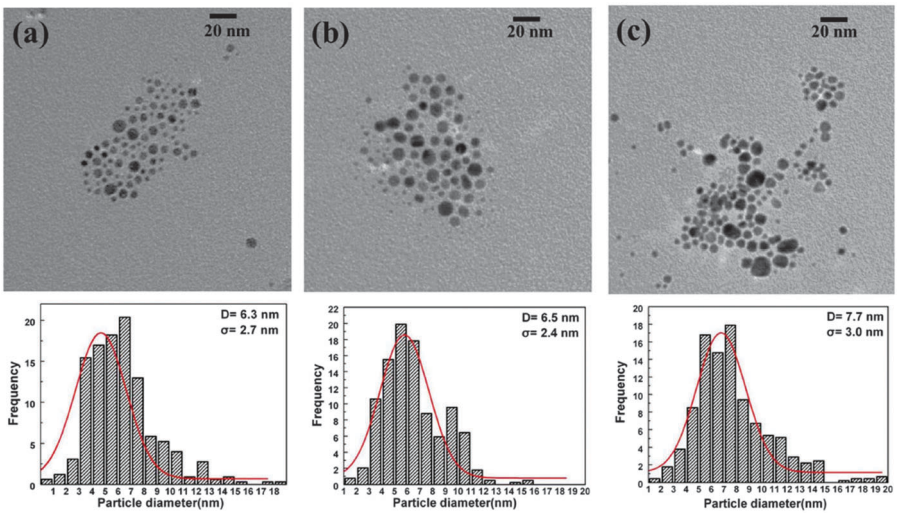

Fig. 2 TEM images and size distribution histograms of Ag NPs prepared from molar concentrations of $AgNO_3$: (a) χ_{Ag} = 0.5 mM, (b) χ_{Ag} = 1.0 mM and (c) χ_{Ag} = 2.0 mM.

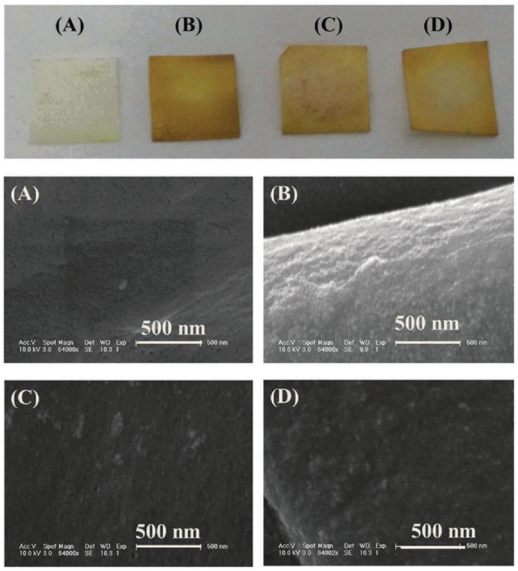

Fig. 3 The pictures and SEM images of grafted PP coated with Ag NPs (0.5 mM): (A) PP-*g*-P (NIPAAm), (B–D) PP-*g*-P(NIPAAm-*co*-APMA) with $M_{NIPAAm:APMA}$ = 2 : 1, 5 : 1 and 10 : 1.

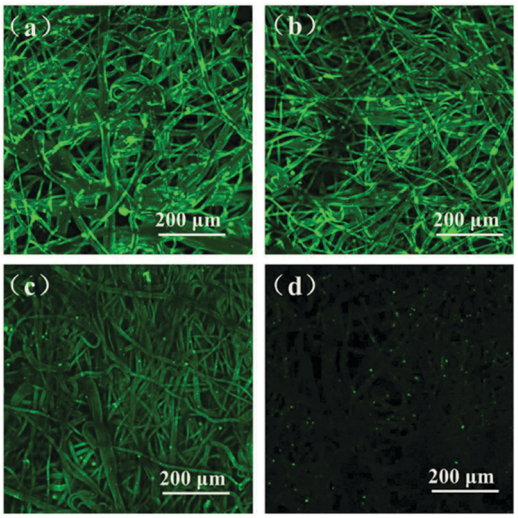

Fig. 4 CLSM images of FITC-Fib adsorption onto (a) virgin PP, (b) Ag NP-loaded surface of virgin PP, (c) PP-*g*-P(NIPAAm-*co*-APMA) and (d) Ag NP-loaded surface of PP-*g*-P(NIPAAm-*co*-APMA).

accessible sites are provided to modify the Ag NPs *via* electrostatic interactions.

3.3 Hemocompatibility of Modified PP Membranes

3.3.1 Protein absorption. Plasma protein absorption has a significant role in the hemocompatibility of biomaterials; this step is the first to occur when the biomaterial surface comes in contact with blood, and thereby subsequently induces platelet and cell adhesion. Fibrinogen (Fib) was used as a model protein to determine the protein adsorption of membranes. Fig. 4 shows FITC-Fib absorption on the surface of virgin and modified PP. An intense fluorescence intensity is observed across the PP surface because of its high hydrophobicity (Fig. 4a). No differences were observed after Ag NP treatment of virgin PP because almost no Ag NPs were loaded on the surface. After grafting with APMA and NIPAAm, the fluorescence intensity decreases because of the hydrophilicity of P (NIPAAm-*co*-APMA) (Fig. 4c). Almost no fluorescence was detected on the surface of the Ag NP-loaded PP-*g*-P (NIPAAm-*co*-APMA) (Fig. 4d). The quantitative data are shown in the ESI† of Fig. S1. The fluorescence intensity of the Ag NP-loaded PP-*g*-P(NIPAAm-*co*-APMA) decreases by 90% for the virgin PP. The isoelectric point of Fib is 5.5; Fib has a negative charge under physiological pH. The positive charge of APMA promotes Fib absorption on the surface of PP-*g*-P (NIPAAm-*co*-APMA). The influence of electrostatic interaction is weakened by the introduction of Ag NPs. These results indicate that Ag NP treatment of grafting PP prevents plasma protein adsorption and neutralizes the surface charge.

3.3.2 Platelet adhesion. Platelet adhesion and then activation on a solid surface is one of the important parameters to evaluate the hemocompatibility of biomaterials.[54] Once plasma protein is adsorbed on the surface of a biomaterial, platelets adhere, spread and aggregate, which ultimately leads to thrombus formation.[55] Fig. 5 shows platelet adhesion on the surface of PP-*g*-P (NIPAAm) and PP-*g*-P(NIPAAm-*co*-APMA) with different monomer ratios and the corresponding Ag NP-loaded surfaces. In Fig. 5a, only a few platelets are visible on the surface of PP-*g*-P (NIPAAm), and the platelets keep their original shape because of the hydration of P(NIPAAm) chains. However, a large number of platelets were found on the surface of PP-*g*-P (NIPAAm-*co*-APMA) (Fig. 5b–d), which is attributed to the electrostatic attraction between the positively charged APMA and the negatively charged platelets. The detailed reason is discussed in our previous work.[40] After adsorption of the Ag NPs, almost no platelets were observed on the surface of the Ag NP-loaded PP membranes (Fig. 5A–D). The positive charges on the membrane surface are neutralized by Ag NPs; thus, the electrostatic interaction between membranes and platelets is diminished. Therefore, Ag NPs deposited on PP membranes have excellent hemocompatibility for resisting platelet adhesion.

3.3.3 Effect of releasing TPGS on erythrocytes. TPGS is synthesized from the lipid-soluble antioxidant α-tocopherol (vitamin E) by grafting onto a polyethylene glycol (PEG) oligomer through a succinate diester linkage. The antioxidant and anti-hemolytic properties of TPGS have been confirmed by various studies.[6,56] Fig. 6 shows the hemolysis rates of PP-*g*-P (NIPAAm) and PP-*g*-P (NIPAAm-*co*-APMA) with different $M_{NIPAAm:APMA}$ and their corresponding Ag NP-loaded surfaces at different time points. Before 12 h, the hemolysis rates of Ag NP-loaded surfaces were slightly higher than those without loaded Ag NPs at $M_{NIPAAm:APMA}$ = 2 : 1 and 5 : 1. After 12 h, the hemolysis rates of the Ag NP-loaded surfaces were much lower than those of the unloaded surfaces. The hemolysis rates increased with time for each sample because oxygen radicals were generated in time, which may cause lipid peroxidation and hemolysis. These results are consistent with our previous work, wherein TPGS from the loaded PP membranes affected hemolysis at different periods.[40] During the early stages of release, TPGS maintained

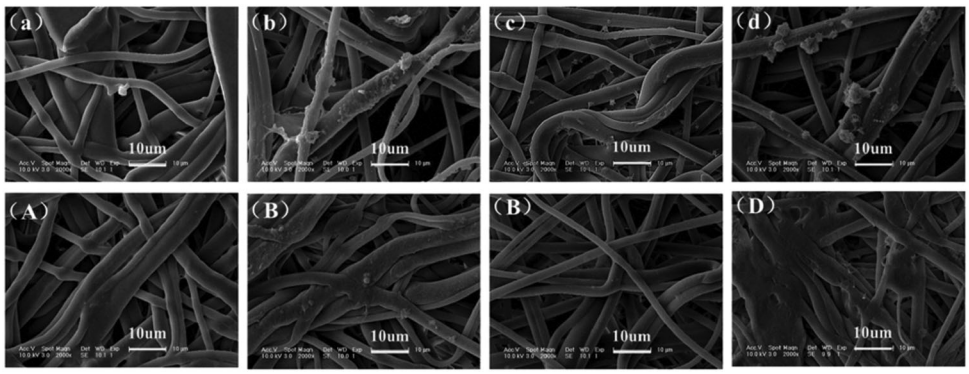

Fig. 5 SEM images of platelets adhered onto the surfaces of (a) PP-*g*-P(NIPAAm), (b–d) PP-*g*-P(NIPAAm-*co*-APMA) with $M_{NIPAAm:APMA}$ = 2 : 1, 5 : 1 and 10 : 1 and Ag NP-loaded surfaces of (A) PP-*g*-P(NIPAAm), (B–D) PP-*g*-P(NIPAAm-*co*-APMA) with $M_{NIPAAm:APMA}$ = 2 : 1, 5 : 1 and 10 : 1.

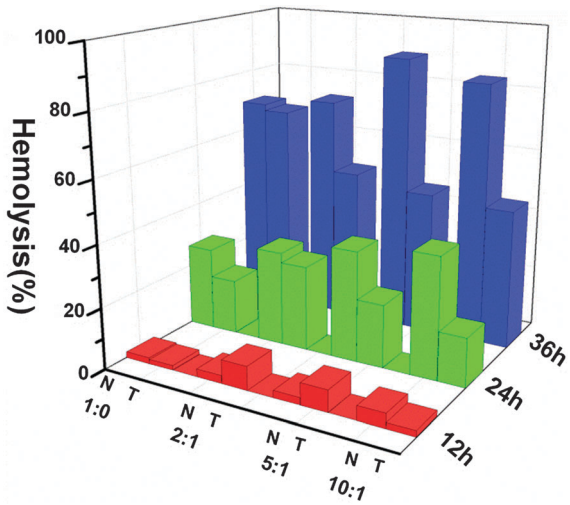

Fig. 6 Hemolysis rates of PP-*g*-P (NIPAAm) (1 : 0) and PP-*g*-P (NIPAAm-*co*-APMA) with $M_{NIPAAm:APMA}$ = 2 : 1, 5 : 1 and 10 : 1 (N) and the corresponding Ag NP-loaded surfaces (T).

the tiny (nanometer-sized) tubers on the membrane surface and enhanced membrane permeabilization by generating nanosize pores on the cell membranes. Subsequently, the incorporated TPGS decreased the lipid peroxidation of erythrocytes and filled the lipid bilayer of these erythrocytes to prevent hemolysis.

The morphological changes of erythrocytes were measured by CLSM after Ag NP-loaded PP membranes came in contact with blood. Fig. 7 shows the CLSM micrographs of erythrocytes which were in contact with PP-*g*-P (NIPAAm) and PP-*g*-P (NIPAAm-*co*-APMA) of different $M_{NIPAAm:APMA}$, as well as the corresponding Ag NP-loaded surfaces. For the unloaded PP membranes (Fig. 7a–d), most erythrocytes were transformed into echinocytes and lost their normal shape. The phospholipids were concentrated into the pointed stars, which appeared brighter than other parts of the erythrocytes. The erythrocyte shape is sensitive to peroxidation by decreasing the fluidity of the lipid bilayer of the membranes. Rice-Evans reported that echinocytes were produced by the peroxide stress of erythrocytes.[57] Most of the erythrocytes on the surfaces of Ag NP-loaded PP maintained their normal discoid shapes and sizes, based on the action of TPGS (Fig. 7A–D). The morphological changes of erythrocytes were also observed by SEM (Fig. S2, ESI†). The result is consistent with the CLSM data. These results proved that TPGS prevents the original morphological changes of RBCs and maintains the normal function of RBCs in blood. Therefore, TPGS endows PP membranes with excellent antioxidant properties.

3.4 Antibacterial test

3.4.1 Bacteria adhesion. The prevention of bacterial adhesion is an extremely important step to prevent bacterial infection. Once bacteria have attached onto a surface, bacteria will rapidly colonize the surface and form biofilms. The antibacterial properties of Ag NP-treated PP were tested with Gram-negative *Escherichia coli* and Gram-positive *Staphylococcus aureus.* The *E. coli* resistance of modified PP is shown in Fig. 8. A few *E. coli* cells were observed on the virgin PP after incubation in PBS for 2 h (Fig. 8a). This result is attributed to the hydrophobicity of PP, which promotes protein absorption and consequently induces the adhesion of *E. coli* (Fig. 4a). Proteins are the most functionally diverse active components that promote bacterial adhesion to a surface.[58] Nevertheless, almost none of the *E. coli* adhered onto the surface of PP-*g*-P(NIPAAm) (Fig. 8b), which can be attributed to the hydration of P(NIPAAm) chains. By contrast, a large number of *E. coli* cells were found on the surface of PP-*g*-P (NIPAAm-*co*-APMA) (Fig. 8c–e), which is also attributed to the electrostatic attraction between the positively charged APMA and the negatively charged bacteria. Henceforth, the anti-bacterial ability of the PP-*g*-P (NIPAAm) sample is superior to that of the other samples when no Ag NPs were loaded. The resistance against *E. coli* of Ag NP-loaded surfaces is presented in Fig. 8 (bottom). No differences were observed between the virgin PP and Ag NP-loaded PP (Fig. 8A). Compared with the unloaded samples, bacteria were almost absent on the surface of Ag NP-loaded PP-*g*-P (NIPAAm-*co*-APMA) (Fig. 8c–e). On the one hand, Ag NP loading eliminated the positive charge on the membrane surface. The electrostatic interaction between the membranes and bacteria decreased after loading. On the other hand, the released silver ions killed the bacteria cells. In addition, the bacteria adhesion of

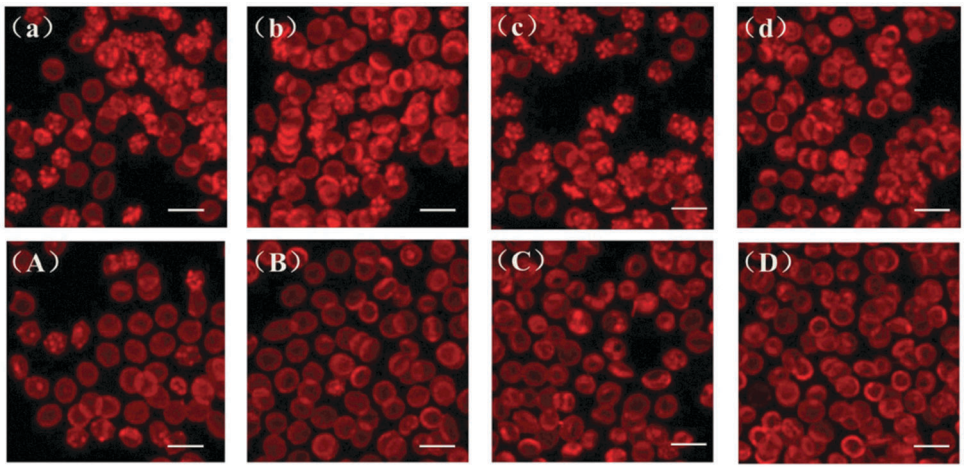

Fig. 7 CLSM images of RBCs of (a) PP-*g*-P(NIPAAm) and (b–d) PP-*g*-P(NIPAAm-*co*-APMA) with $M_{NIPAAm:APMA}$ = 2 : 1, 5 : 1 and 10 : 1 and Ag NP-loaded surface of (A) PP-*g*-P(NIPAAm), and (B–D) PP-*g*-P(NIPAAm-*co*-APMA) with $M_{NIPAAm:APMA}$ = 2 : 1, 5 : 1 and 10 : 1.

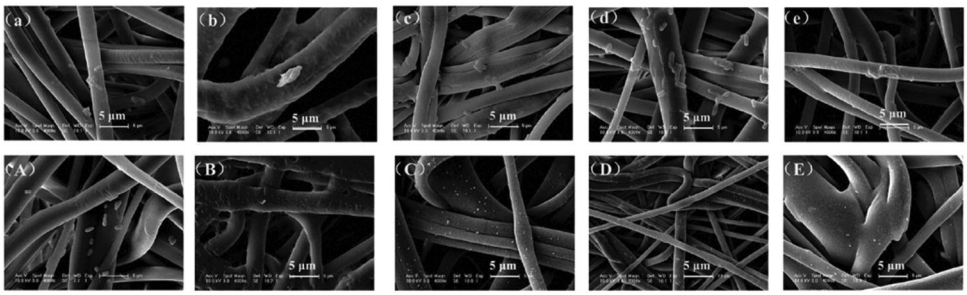

Fig. 8 SEM images of *E. coli* adhered onto the surface of (a) PP, (b) PP-*g*-P(NIPAAm), (c–e) PP-*g*-P(NIPAAm-*co*-APMA) with $M_{NIPAAm:APMA}$ = 2 : 1, 5 : 1 and 10 : 1, and onto the Ag NP-loaded surface of (A) PP, (B) PP-*g*-P(NIPAAm), (C–E) PP-*g*-P(NIPAAm-*co*-APMA) with $M_{NIPAAm:APMA}$ = 2 : 1, 5 : 1 and 10 : 1.

S. aureus is shown and discussed in Fig. S3a–d (ESI†). The surface of Ag NP-loaded PP-*g*-P (NIPAAm-*co*-APMA) also had excellent anti-bacteria adhesion properties against *S. aureus*. The bacteria adhesion results indicate that Ag NPs on the surface prevent bacterial adhesion at the early stages.

3.4.2 Bactericidal activity. Antibacterial testing of the virgin and modified PP was conducted *via* bactericidal activity assays. Fig. 9A shows the bacterial colony forming units (CFU) of *E. coli* grown on culture plates for the virgin and modified PP. The plates of virgin PP (Fig. 9a) and the Ag NP-loaded virgin PP (Fig. 9b) are covered with a higher density of bacterial colonies. The number of bacterial colonies on the surface of PP-*g*-P (NIPAAm-*co*-APMA) strongly increased because of the electrostatic interaction. However, the Ag NP-loaded surface of PP-*g*-P (NIPAAm-*co*-APMA) can efficiently inhibit the growth of *E. coli*. The quantitative data are shown in Fig. 9B. Compared with virgin PP,

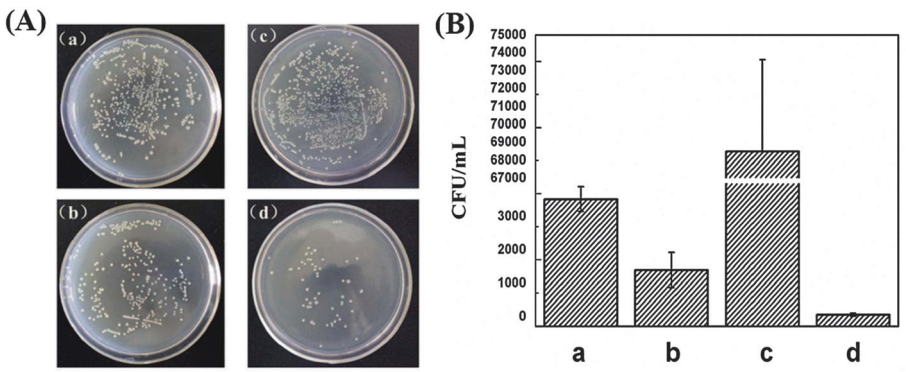

Fig. 9 (A) Photographs of agar plates corresponding to the *E. coli* suspension recovered from (a) virgin PP, (b) Ag NP-loaded surface of virgin PP, (c) PP-*g*-P (NIPAAm-*co*-APMA) and (d) Ag NP-loaded surface of PP-*g*-P (NIPAAm-*co*-APMA). (B) The corresponding quantitative data from the bacteria colony count method.

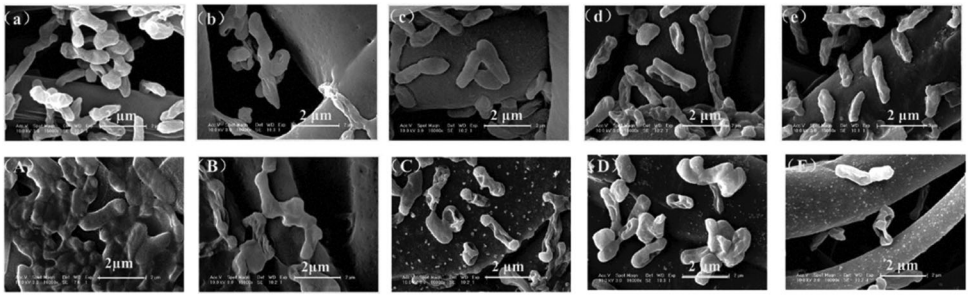

Fig. 10 SEM images of *E. coli* incubated on the surface for 24 h of (a) PP, (b) PP-*g*-P(NIPAAm), (c–e) PP-*g*-P(NIPAAm-*co*-APMA) with $M_{NIPAAm:APMA}$ = 2 : 1, 5 : 1 and 10 : 1, and of the Ag NP-loaded surface of (A) PP, (B) PP-*g*-P(NIPAAm), (C–E) PP-*g*-P(NIPAAm-*co*-APMA) with $M_{NIPAAm:APMA}$ = 2 : 1, 5 : 1 and 10 : 1.

a 98.4% reduction of *E. coli* is observed for the Ag NP-loaded surface of PP-*g*-P (NIPAAm-*co*-APMA). Compared with the unloaded PP-*g*-P (NIPAAm-*co*-APMA), the density of *E. coli* cells on the surface of an Ag NP-loaded sample was reduced by almost 99.9%. Furthermore, almost no bacterial colonies appeared on the plate after the *S. aureus* suspension was contacted with the Ag NP-loaded PP-*g*-P (NIPAAm-*co*-APMA) (Fig. S4, ESI†). The density of *S. aureus* cells on the Ag NP-loaded sample was reduced by 100%, compared with the unloaded sample. These abovementioned results clearly demonstrate that the biocidal activity of the Ag NP-loaded sample increased because of the introduction and release of Ag NPs; almost all of the bacterial contaminants were killed. The bacterial inhibition of Ag NPs is caused by the direct nanoscale contact with the silver surface and the Ag^+ release mechanism.[44] A combination of these two processes leads to the disruption of the cell membrane and strong bactericidal action. First, the Ag NPs attach to the surface of the cell membrane and disturb its main functionalities, such as the permeability and respiration process. Taglietti *et al.* investigated the mechanism of antibacterial activity of Ag NPs that were grafted onto thiol-functionalized glass surfaces on Gram-negative and Gram-positive bacterial model strains.[44] After contact with the treated surface, the cell membranes were completely disrupted with evidence of cellular damage. Second, the released Ag^+ from Ag NPs could lead to the inhibition of phosphate uptake, as well as the loss of phosphate, and some amino acids like glutamine or proline *via* leakage from *E. coli* cells.[59] These results clearly indicate that the surface loading of Ag NPs is a powerful method to substantially prevent the adherence of bacteria and enhance the antibacterial property of the PP membrane.

3.4.3 Biofilm formation. The most promising anti-adhesive surface modifications prevent the initial adhesion of bacteria, but a small number of bacteria cells still form a mature biofilm.[60] The biofilm itself can filter out antibiotics or secrete factors that reduce the antibiotic concentration within the biofilm, thereby rendering conventional oral, topical or intravenous antibacterial treatments inadequate.[61] The effectiveness of Ag NP-loaded PP in inhibiting biofilm formation was assessed after incubation in a growth medium containing 10^6 cells per mL for 24 h at 37 °C. As shown in Fig. 10, bacteria formed biofilms on the virgin PP (Fig. 10a) and Ag NP-treated virgin PP (Fig. 10A). The bacteria in these samples revealed intact cells and featured undamaged membranes. For PP-*g*-P (NIPAAm-*co*-APMA) (Fig. 10c–e), some bacteria exhibited membrane wrinkling across the entire cell surface because of the positive charge of APMA.[62] By contrast, most of the bacterial cells were dead on the surface of Ag NP-loaded PP-*g*-P (NIPAAm-*co*-APMA) (Fig. 10c–e). The cell membranes were completely disrupted, with evidence of cellular damage. Numerous holes on the bacterial surface caused the leakage of intracellular molecules such as ATP. The quantitative data showed (Fig. 11) the bactericidal efficiency based on the *E. coil* morphology. Only 5% of the bacteria were dead on the surface of the virgin PP and the Ag NP-treated virgin PP. By contrast, 93% of the *E. coli* were killed on the surface of the Ag NP-loaded PP-*g*-P (NIPAAm-*co*-APMA) with a molar ratio of $M_{NIPAAm:APMA}$ = 5 : 1. For Gram-positive *S. aureus*, Ag NP-loaded samples also presented excellent resistance against the formation of biofilms (Fig. S3A–D, ESI†). The above results indicate that the Ag NP-loaded on the surface of modified PP can efficiently inhibit the formation of biofilms and kill most of the bacteria on the grafted PP surface.

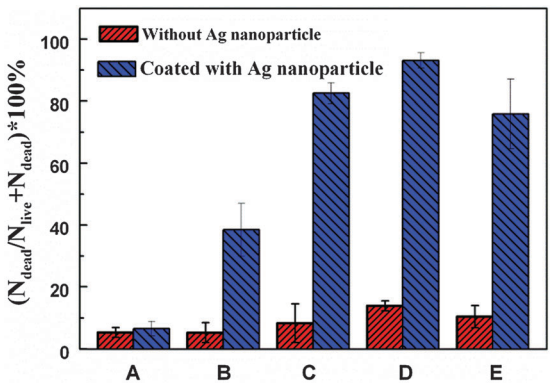

Fig. 11 Bactericidal efficiency of the membrane without Ag NP-loaded (red) and coated with Ag NPs (blue) of (A) virgin PP (B) PP-*g*-P(NIPAAm) and (C–E) PP-*g*-P(NIPAAm-*co*-APMA) with $M_{NIPAAm:APMA}$ = 2 : 1, 5 : 1 and 10 : 1.

4. Conclusion

Ag NPs were synthesized in the presence of carboxylic TPGS for the first time, to the best of our knowledge. The UV-visible spectroscopy, transmission electron microscopy, and zeta potential measurements confirmed that the Ag NPs were well dispersed in the solution because of the negative charge

rendered by TPGS. The Ag NPs were loaded on the surface of PP-*g*-P (NIPAAm-*co*-APMA) through electrostatic interactions between the negatively charged Ag NPs and the positively charged APMA brushes. The Ag NP-loaded PP-*g*-P (NIPAAm-*co*-APMA) membranes had excellent hemocompatibility for resisting platelet adhesion. TPGS decreased hemolysis, prevented the original morphology changes of RBCs, and maintained the normal function of RBCs in blood. Thus, TPGS endowed membranes with excellent antioxidant properties. The Ag NPs loaded on the surface prevented bacterial adhesion during the early stages and inhibited the formation of biofilms. Overall, TPGS is a promising surfactant for synthesizing metal nanomaterials because of its low human health risk, effectiveness as a dispersant and antioxidative property. The proposed method is suitable for producing hemocompatible biomaterials with simultaneous antioxidative and antibacterial properties in a surface-independent manner.

Acknowledgements

The authors acknowledge the financial support of the National Science Foundation of China (Project No. 51303178 and 21274150).

References

1 Y. Li, C. M. Santos, A. Kumar, M. Zhao, A. I. Lopez, G. Qin, A. M. McDermott and C. Cai, *Chemistry*, 2011, **17**, 2656–2665.
2 Z. Zhang, M. Zhang, S. Chen, T. A. Horbetta, B. D. Ratner and S. Jiang, *Biomaterials*, 2008, **29**, 4285–4291.
3 G. A. Abraham, A. A. A. de Queiroz and J. S. Román, *Biomaterials*, 2002, **23**, 1625–1638.
4 S. Mansouri, Y. Merhi, F. M. Winnik and M. Tabrizian, *Biomacromolecules*, 2011, **12**, 585–592.
5 P. Pleonsil, S. Soogarun and Y. Suwanwong, *Int. J. Biol. Macromol.*, 2013, **60**, 393–398.
6 G. J. Dahe, R. S. Teotia, S. S. Kadam and J. R. Bellare, *Biomaterials*, 2011, **32**, 352–365.
7 C. M. Teng, G. Hsiao, F. N. Ko, D. T. Lin and S. S. Lee, *Eur. J. Pharmacol.*, 1996, **303**, 129–139.
8 V. Martínez, V. Ugartondo, M. P. Vinardell, J. L. Torres and M. Mitjans, *J. Agric. Food Chem.*, 2012, **60**, 4090–4095.
9 V. Ugartondo, M. Mitjans, J. L. Torres and M. P. Vinardell, *J. Agric. Food Chem.*, 2009, **57**, 4459–4465.
10 L. N. Grinberg, H. Newmark, N. Kitrossky, E. Rahamim, M. Chevion and E. A. Rachmilewitz, *Biochem. Pharmacol.*, 1997, **54**, 973–978.
11 B. A. Wagner, G. R. Buettner and C. P. Burns, *Arch. Biochem. Biophys.*, 1996, **334**, 261–267.
12 M. Sasaki, *J. Artif. Organs*, 2006, **9**, 50–60.
13 K.-i. Yamamoto, M. Matsuda, M. Okuoka, T. Yakushiji, M. Fukuda, T. Miyasaka, Y. Matsumoto and K. Sakai, *J. Membr. Sci.*, 2007, **302**, 115–118.
14 Z. Zhang, S. Tan and S. S. Feng, *Biomaterials*, 2012, **33**, 4889–4906.
15 X. Zeng, W. Tao, L. Mei, L. Huang, C. Tan and S. S. Feng, *Biomaterials*, 2013, **34**, 6058–6067.
16 J. Pan and S. S. Feng, *Biomaterials*, 2009, **30**, 1176–1183.
17 Z. Zhang and S. S. Feng, *Biomaterials*, 2006, **27**, 262–270.
18 Z. Zhang, S. Huey Lee and S. S. Feng, *Biomaterials*, 2007, **28**, 1889–1899.
19 J. W. Costerton, P. S. Stewart and E. P. Greenberg, *Science*, 1999, **284**, 1318–1322.
20 K. Glinel, A. M. Jonas, T. Jouenne, J. Leprince, L. Galas and W. T. S. Huck, *Bioconjugate Chem.*, 2008, **20**, 71–77.
21 O. Azzaroni, *J. Polym. Sci., Part A: Polym. Chem.*, 2012, **50**, 3225–3258.
22 M. R. Nejadnik, H. C. van der Mei, W. Norde and H. J. Busscher, *Biomaterials*, 2008, **29**, 4117–4121.
23 N. Blanchemain, T. Laurent, F. Chai, C. Neut, S. Haulon, V. Krump konvalinkova, M. Morcellet, B. Martel, C. J. Kirkpatrick and H. F. Hildebrand, *Acta Biomater.*, 2008, **4**, 1725–1733.
24 J. H. Park, K. B. Lee, I. C. Kwon and Y. H. Bae, *J. Biomater. Sci., Polym. Ed.*, 2001, **12**, 629–645.
25 M. A. Qureshi and F. Khatoon, *Polym.-Plast. Technol. Eng.*, 2015, **54**, 573–580.
26 Z. L. Zhang, Z. C. Wang, J. Nong, C. A. Nix, H. F. Ji and Y. H. Zhong, *Biofabrication*, 2015, **7**, 1–13.
27 J. M. Schierholz and G. Pulverer, *Biomaterials*, 1998, **19**, 2065–2074.
28 D. Campoccia, L. Montanaro, P. Speziale and C. R. Arciola, *Biomaterials*, 2010, **31**, 6363–6377.
29 D. H. Duckworth and P. A. Gulig, *BioDrugs*, 2002, **16**, 57–62.
30 J. Klem, D. Domotor, G. Schneider, T. Kovacs, A. Toth and G. Rakhely, *Acta Microbiol. Immunol. Hung.*, 2013, **60**, 411–422.
31 K. Meczker, D. Domotor, J. Vass, G. Rakhely, G. Schneider and T. Kovacs, *FEMS Microbiol. Lett.*, 2014, **350**, 25–27.
32 J. S. Kim, E. Kuk, K. N. Yu, J. H. Kim, S. J. Park, H. J. Lee, S. H. Kim, Y. K. Park, Y. H. Park, C. Y. Hwang, Y. K. Kim, Y. S. Lee, D. H. Jeong and M. H. Cho, *Nanomed.: Nanotechnol., Biol. Med.*, 2007, **3**, 95–101.
33 C. Marambio Jones and E. M. V. Hoek, *J. Nanopart. Res.*, 2010, **12**, 1531–1551.
34 M. Rai, A. Yadav and A. Gade, *Biotechnol. Adv.*, 2009, **27**, 76–83.
35 L. Liu, J. Yang, J. Xie, Z. Luo, J. Jiang, Y. Y. Yang and S. Liu, *Nanoscale*, 2013, **5**, 3834–3840.
36 J. D. Padmos, R. T. M. Boudreau, D. F. Weaver and P. Zhang, *Langmuir*, 2015, **31**, 3745–3752.
37 W.-R. Li, X.-B. Xie, Q.-S. Shi, H.-Y. Zeng, Y.-S. Ou-Yang and Y.-B. Chen, *Appl. Microbiol. Biotechnol.*, 2010, **85**, 1115–1122.
38 I. Sondi and B. Salopek Sondi, *J. Colloid Interface Sci.*, 2004, **275**, 177–182.
39 A. Dror Ehre, H. Mamane, T. Belenkova, G. Markovich and A. Adin, *J. Colloid Interface Sci.*, 2009, **339**, 521–526.
40 E. Amato, Y. A. Diaz Fernandez, A. Taglietti, P. Pallavicini, L. Pasotti, L. Cucca, C. Milanese, P. Grisoli, C. Dacarro, J. M. Fernandez Hechavarria and V. Necchi, *Langmuir*, 2011, **27**, 9165–9173.
41 E. I. Alarcon, K. Udekwu, M. Skog, N. L. Pacioni, K. G. Stamplecoskie, M. González Béjar, N. Polisetti, A. Wickham,

A. Richter Dahlfors, M. Griffith and J. C. Scaiano, *Biomaterials*, 2012, **33**, 4947–4956.
42 A. J. Kora, R. Manjusha and J. Arunachalam, *Mater. Sci. Eng., C.*, 2009, **29**, 2104–2109.
43 M. A. Hoppens, C. B. Sylvester, A. T. Qureshi, T. Scherr, D. R. Czapski, R. S. Duran, P. B. Savage and D. Hayes, *ACS Appl. Mater. Interfaces*, 2014, **6**, 13900–13908.
44 A. Taglietti, Y. A. Diaz Fernandez, E. Amato, L. Cucca, G. Dacarro, P. Grisoli, V. Necchi, P. Pallavicini, L. Pasotti and M. Patrini, *Langmuir*, 2012, **28**, 8140–8148.
45 C. Li, J. Jin, J. Liu, X. Xu and J. Yin, *ACS Appl. Mater. Interfaces*, 2014, **6**, 13956–13967.
46 V. Dupres, C. Verbelen and Y. F. Dufrêne, *Biomaterials*, 2007, **28**, 2393–2402.
47 N. R. Jana, L. Gearheart and C. J. Murphy, *Chem. Commun.*, 2001, 617–618.
48 J. Yang, J. Y. Lee, L. X. Chen and H. P. Too, *J. Phys. Chem. B*, 2005, **109**, 5468–5472.
49 J. J. Mock, M. Barbic, D. R. Smith, D. A. Schultz and S. Schultz, *J. Chem. Phys.*, 2002, **116**, 6755–6759.
50 I. Pastoriza-Santos and L. M. Liz-Marzán, *Langmuir*, 1999, **15**, 948–951.
51 A. B. Smetana, K. J. Klabunde, G. R. Marchin and C. M. Sorensen, *Langmuir*, 2008, **24**, 7457–7464.
52 E. T. Hwang, J. H. Lee, Y. J. Chae, Y. S. Kim, B. C. Kim, B. I. Sang and M. B. Gu, *Small*, 2008, **4**, 746–750.
53 K. K. Goli, N. Gera, X. Liu, B. M. Rao, O. J. Rojas and J. Genzer, *ACS Appl. Mater. Interfaces*, 2013, **5**, 5298–5306.
54 H. T. Spijker, R. Bos, H. J. Busscher, T. G. van Kooten and W. van Oeveren, *Biomaterials*, 2002, **23**, 757–766.
55 C. Li, J. Jin, J. Liu, X. Xu and J. Yin, *RSC Adv.*, 2014, **4**, 24842–24851.
56 Q. Shi, X. Xu, Q. Fan, J. Hou, W. Ye and J. Yin, *J. Mater. Chem. B*, 2015, **3**, 2119–2126.
57 P. P. Constantinides, J. H. Han and S. S. Davis, *Pharm. Res.*, 2006, **23**, 243–255.
58 S. Yuan, J. Zhao, S. Luan, S. Yan, W. Zheng and J. Yin, *ACS Appl. Mater. Interfaces*, 2014, **6**, 18078–18086.
59 M. Yamanaka, K. Hara and J. Kudo, *Appl. Environ. Microbiol.*, 2005, **71**, 7589–7593.
60 A. K. Muszanska, E. T. J. Rochford, A. Gruszka, A. A. Bastian, H. J. Busscher, W. Norde, H. C. van der Mei and A. Herrmann, *Biomacromolecules*, 2014, **15**, 2019–2026.
61 M. C. Coll Ferrer, N. J. Hickok, D. M. Eckmann and R. J. Composto, *Soft Matter*, 2012, **8**, 2423–2431.
62 S. B. Lee, R. R. Koepsel, S. W. Morley, K. Matyjaszewski, Y. Sun and A. J. Russell, *Biomacromolecules*, 2004, **5**, 877–882.

